Ordered polythiophene/fullerene composite core–shell nanorod arrays for solar cell applications

Hsu-Shen Wang[1]**, Li-Hua Lin**[1]**, Shih-Yung Chen**[2]**, Yuh-Lin Wang**[2,3] **and Kung-Hwa Wei**[1]

[1] Department of Materials Science and Engineering, National Chiao Tung University, 1001 Ta Hsueh Road, Hsinch 30050, Taiwan, Republic of China
[2] Institute of Atomic and Molecular Science, Academia Sinica, PO Box 23-166, Taipei 106, Taiwan, Republic of China
[3] Department of Physics, National Taiwan University, Taipei 106, Taiwan, Republic of China

E-mail: khwei@mail.nctu.edu.tw

Abstract
For the first time, we have used melt-assisted wetting of porous alumina templates to prepare ordered core–shell nanorod arrays of poly(3-hexylthiophene) (P3HT) and [6,6]-phenyl-C_{61}-butyric acid methyl ester (PCBM) for use in polymer solar cells. We characterized these arrays using tunneling electron microscopy and conductance atomic force microscopy, which revealed the presence of phase-separated shell (p-type) and core (n-type) regions. Under illumination, we observed a variation of several picoamperes between the currents in the core and shell regions of the P3HT/PCBM nanorod arrays.

(Some figures in this article are in colour only in the electronic version)

1. Introduction

The development of conjugated polymers for use in organic optoelectronic devices has advanced dramatically in recent years. In particular, polymer heterojunction solar cell devices are receiving considerable attention [1–7]. Typically, the active layer of a polymer heterojunction solar cell is prepared from a thin film of an electron-donating conjugated polymer and an electron-accepting species. The power conversion efficiency (PCE) of polymer heterojunction solar cells has improved dramatically over the last few years; those containing blends of regioregular poly(3-hexylthiophene) (P3HT) and [6,6]-phenyl-C_{61}-butyric acid methyl ester (PCBM), have recently reached PCEs of approx. 4–5% under standard solar conditions (AM 1.5G, 100 mW cm^{-2}) [8–10].

There is generally no preferred direction for the internal fields of separated charges for a polymer heterojunction solar cell device; that is, the electrons and holes created within the volume have no net resulting direction in which they should move [11]. Furthermore, because the separated holes and electrons require percolated pathways for transport to their contacts, device structures containing a two-phase donor/acceptor film must exhibit features interspaced with an average length of approx. 10–20 nm, equal to or less than the exciton diffusion length. This structure minimizes the losses that arise from the recombination of charges moving in the wrong direction.

The wetting of porous alumina membrane (AAO) templates with polymer melts, solutions or polymer-containing mixtures is a simple and versatile method for the fabrication of one-dimensional structures having diameters ranging from a few tens of nanometers to several micrometers. This approach is a promising one for preparing functionalized nanorod–template hybrid systems, and free-standing nanotubes and nanorods [12–15]. Additionally, the hole mobility of a pure P3HT nanowire in a straight AAO pore is enhanced by as much as a factor of 20 compared with that in a neat film [16] because the polymer chains are partially aligned in the charge transport direction after infiltrating the vertically straight nanopores of the anodic alumina. Therefore, in this present study, we used the wetting of ordered AAO templates to fabricate (figure 1) P3HT/PCBM core–shell nanorods for use in solar cell devices. We expect that such ordered nanorod structures will provide more efficient polymer solar cells.
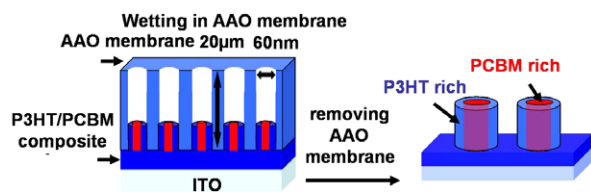
Figure 1. Cartoon representation of the well-ordered nanorod structures.

Figure 2. (a) SEM image of the P3HT/PCBM (1:1, w/w) nanorod array; the inset displays the ordered Al membrane (scale bar: 100 nm). (b) Top-view TEM image of the P3HT/PCBM (1:4, w/w) nanorod structure (scale bar: 50 nm).

2. Experimental details

We prepared P3HT/PCBM films having a thickness of 120 nm through solution casting onto ITO glass slides and then placed an alumina membrane (AAO) on top of the P3HT/PCBM film. This P3HT/PCBM film/alumina membrane was sandwiched between two glass slides and then placed in an oven and annealed under vacuum. After 6 h, the assembled system was cooled to room temperature. Dissolving the alumina membranes in 10 wt% NaOH solution released the P3HT/PCBM core–shell nanorod structures, which were dried under vacuum for 12 h prior to characterization. Scanning electron microscopy (SEM) images of the resultant P3HT/PCBM nanostructures were investigated using a JEOL 6500 model scanning electron microscope at an accelerating voltage of 15 kV. The samples were coated with a thin layer of platinum (thickness approx. 3 nm) prior to SEM imaging. Transmission electron microscopy (TEM) images were obtained using an Hitachi H-600 transmission electron microscope. The sample for TEM analysis was prepared by removing the nanorod array thin film from the ITO substrate with 1% HF, and then collecting the thin film with a TEM grid coated with carbon. We performed conductance atomic force microscopy (C-AFM) experiments using platinum-coated silicon cantilevers [NanoSensors Inc. (PPP-ContPt, spring constant $k = 0.2$ N m^{-1})] and a Digital Nanoscope IV operated under ambient conditions. The current density–voltage (J–V) characteristics of the polymers were measured using devices having the structure ITO/PEDOT:PSS/P3HT:PCBM/Al. The ITO-coated glass substrate was pre-cleaned and treated with oxygen plasma prior to use. The P3HT/PCBM layer was spin-coated from a chlorobenzene solution. Using a base pressure below 1×10^{-6} Torr, a layer of Al (100 nm) was vacuum-deposited as the cathode. Testing of the devices was performed under simulated AM 1.5G irradiation (100 mW cm^{-2}) using a xenon lamp-based Newport 66902 150W solar simulator equipped with an AM1.5 filter as the white light source; the optical power at the sample was 100 mW cm^{-2}, detected using an OPHIR thermopile 71964. The current density–voltage (J–V) characteristics were measured using a Keithley 236 source-measure unit.

3. Result and discussion

Figure 2(a) displays an SEM image of the P3HT/PCBM (1:1, w/w) nanorod array structure. The average diameter of the nanorods was approx. 65 nm, equal to the diameter of the nanopores (65 nm) in the ordered AAO membrane (inset to
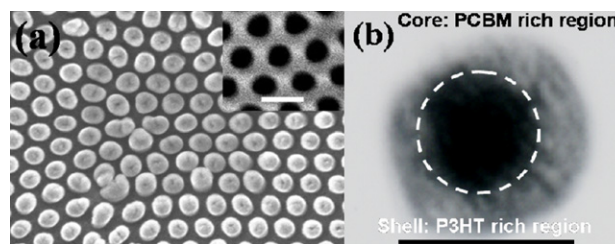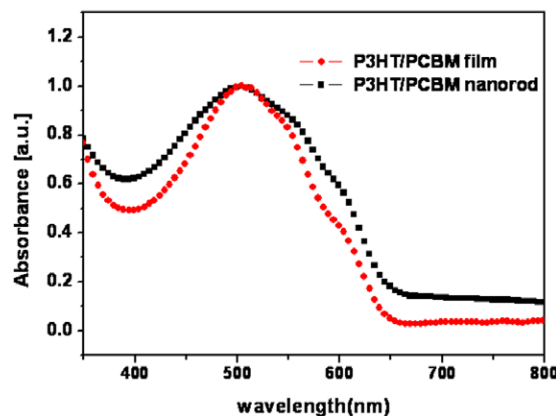

Figure 3. UV spectra of P3HT/PCBM(1:1, w/w) as-cast film (circle) and nanorod structures (square).

figure 2(a)). Figure 2(b) provides a TEM top-view image of the P3HT/PCBM (1:4, w/w) nanorods, revealing their core–shell-like structures; the dark central region of the nanorods represents the PCBM-rich region, which has a higher electron density than that of the P3HT-rich region.

Intensity normalized absorption spectrum of P3HT/PCBM (1:1, w/w) thin film and nanorods are shown in figure 3. The maximum absorption ($\lambda_{\max}$) took place at approx. 504 nm for the P3HT/PCBM thin film, resulting from π–π^* transitions. In comparison, the absorption peak of the P3HT/PCBM nanorod array shifted slightly towards a longer wavelength at 508 nm, as displayed. The full width at half-maximum (FWHM) increased to 231 nm for the P3HT/PCBM nanorod array from 173 nm for the P3HT/PCBM thin film, an increase of 58 nm.

Figure 4 displays C-AFM images of the P3HT/PCBM (1:1, w/w) nanorods embedded onto the ITO glass substrate. In the topographic image (figure 4(a)), the light regions having a height of approx. 70 nm represent the P3HT/PCBM nanorods. In the current image (figure 4(b)), measured at a sample bias of -1 V, the currents of the P3HT/PCBM nanorods (light regions) were approx. 30 pA, whereas those of the spaces between the rods (dark regions) were at the level of the noise (approx. 0.5 pA); this image also reveals the contrast between the current images of the core and shell regions. The current resulted mainly from hole transport because Pt and ITO have high work functions of approx. 5.7 and 4.8 eV, respectively. Because the Pt-coated tip was biased, the influence of the surface electrical properties of
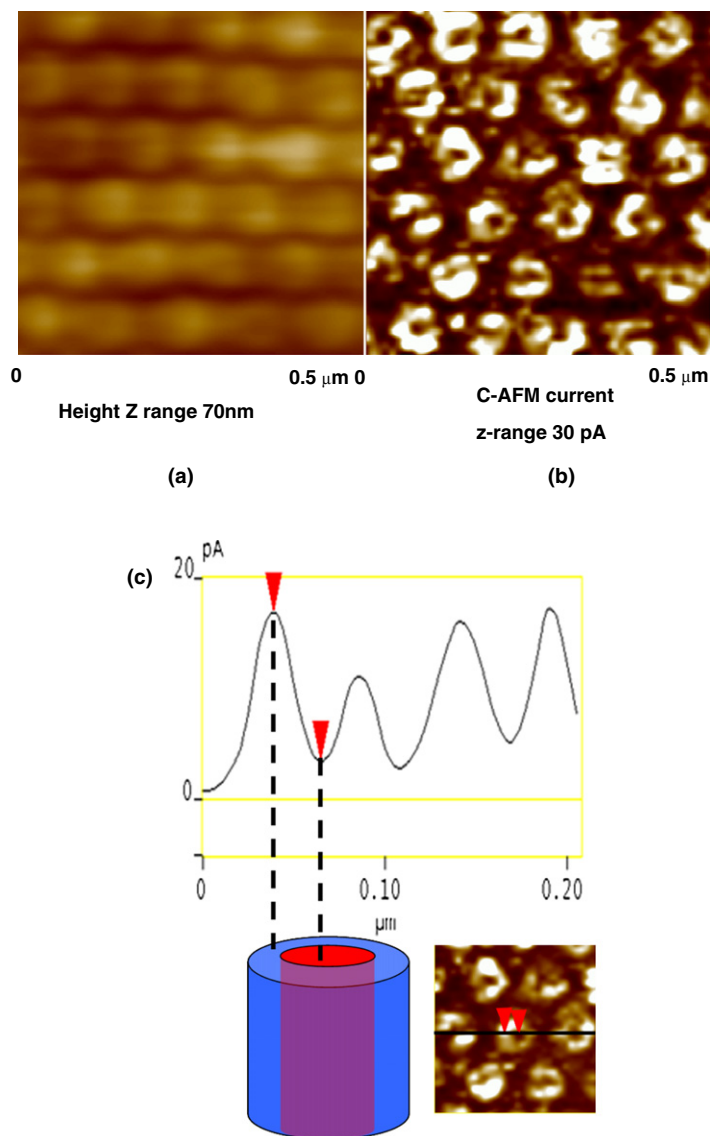
Figure 4. C-AFM (a) topographic vertical distance: 70 nm and (b) current images of a thin film of P3HT/PCBM nanorods. The variation in current between the labeled core (PCBM-rich region) and shell (P3HT-rich region) regions was 14.3 pA.

ITO played only a minor role [17]. We observed a variation in current of 14.3 pA between the charge transport of the core and shell regions of the nanorods, despite having some inhomogeneities in their compositions. This phenomenon resulted primarily from the composition difference between the core and shell region, where the dark central region of the nanorods represents the PCBM-rich region and the light region of the nanorods represents the P3HT-rich region. The nanorods of the P3HT/PCBM blend possessed core–shell structures, with the P3HT-rich regions of the shell evident in the C-AFM current image. Therefore, we expected most of the electron/hole pairs to separate at the p–n interface, such that the electron and hole transport would occur through the PCBM-rich region (n-type) and P3HT-rich region (p-type) individually and efficiently in this core–shell structure.

The phase separation of P3HT/PCBM blends in the wetting of the ordered porous AAO membrane is determined by the flow-induced shear stress, which is the largest along the AAO pore wall and the lowest in the center of the AAO pore.

Since the modulus of PCBM is larger than that of P3HT at 120°, the maximum stress along the AAO pore wall will induce a lower viscosity part of the blend, i.e. P3HT-rich region, to flow along, whereas the minimum stress in the center of the AAO pore will have a higher viscosity part of the blend, PCBM-rich region, to flow along. Consequently, this phase separation of the P3HT/PCBM blend during flow results in core–shell structured nanorods after quenching to room temperature.

Figure 5 displays the J–V characteristics of solar cell devices incorporating ordered nanorods of various compositions. The performance increased upon decreasing the PCBM content (table 1). For the device containing P3HT and PCBM at a 1:2 ratio (w/w), the values of the short-circuit current density (J_{sc}), the fill factor (FF) and the PCE were 4.4 mA cm^{-2}, 38% and 0.66%, respectively; these values increased to 5.9 mA cm^{-2}, 53% and 1.30%, respectively, for the 1:0.6 (w/w) P3HT/PCBM device. This improvement in efficiency might be caused by more efficient
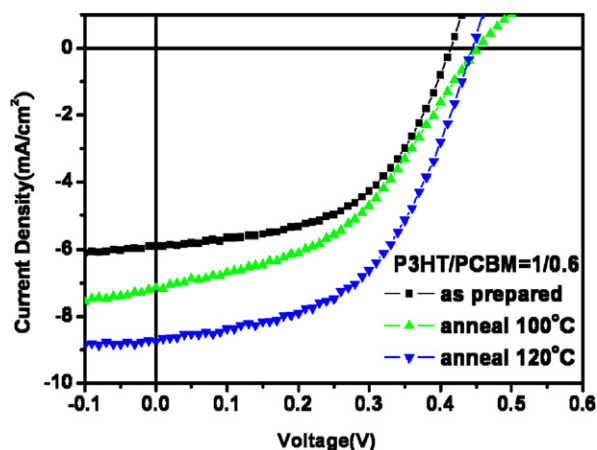
Figure 5. $J-V$ characteristics of P3HT/PCBM nanorod array devices prepared after annealing at various temperatures, measured under AM1.5G illumination at an intensity of 100 mW cm^{-2}.

Table 1. Electronic parameters of vertical p–n junction structure devices prepared from various P3HT/PCBM weight ratios and annealed at various temperatures.

P3HT/PCBM ratio	J_{sc}a (mA cm^{-2})	V_{oc}b (V)	FFc (%)	ηd (%)	Annealing temperaturee (°C)
1:0.6	5.9	0.41	53	1.30	—
1:1	5.8	0.42	35	0.85	—
1:2	4.4	0.40	38	0.66	—
1:0.6	7.2	0.45	45	1.43	100
1:0.6	8.7	0.46	50	2.00	120

[a] Short-circuit current density.
[b] Open-circuit voltage.
[c] Fill factor.
[d] Power conversion efficiency.
[e] Annealing time: 10 min.

charge transport in the device structure, due to the high difference in their composition of core and shell. To improve the performance of our solar cell devices, we subjected them to annealing at various temperatures. For the device incorporating P3HT/PCBM at a 1:0.6 ratio (w/w), the values of PCE and J_{sc} improved to 2.0% (from 1.3%) and 8.7 mA cm^{-2} (from 5.9 mA cm^{-2}), respectively, after thermal annealing at 120 °C for 10 min. We have tried two different annealing temperatures, 100 and 120°C, for the annealing device and it appears that the phase separation of the nanorods at the higher temperature became more complete, leading to a better photovoltaic performance. This improved performance after annealing quite possibly resulted from increases in the degree of crystallization [18], the transport properties [19] and the light absorption [20] of the P3HT-rich region and also from the improved contact at the electrode for the transfer of electrons.

Our P3HT/PCBM devices are actually ordered bulk heterojunction devices. What we are suggesting here is that we can have nanorods with better phase-separated P3HT/PCBM blends, although the boundary between the core–shell structured P3HT/PCBM nanorods is not exactly sharp yet; the wall is the P3HT-rich region and the center is the PCBM-rich region. Moreover, we have different work functions for the front aluminum electrode and the back ITO/PEDOT:PSS electrode, and this barrier height difference will determine the transport direction of electrons and holes in the devices. Since the Al/P3HT barrier height is higher than that of the Al/PCBM, the extraction efficiency of electrons from the Al/PCBM interface is better than from the Al/P3HT interface. Hence, even if we have a vertical p–n junction, electrons tend to travel to the aluminum electrode, and holes tend to travel to the back ITO/PEDOT:PSS electrode, producing a photovoltaic effect.

The area covered by the nanorods on the substrate determines the amount of incident light absorbed. In our devices, this area was approx. 43% (defined by the AAO membrane) of the total substrate surface. Hence, increasing the packing density of the nanorods so that they occupy a greater percentage of the surface area might improve the devices' performance further so that they would have potential for use in solar cell applications.

4. Conclusion

In summary, we have used the melt-assisted wetting of porous alumina templates to fabricate vertical nanorod arrays of P3HT and PCBM having core–shell nanostructures for application in polymer solar cells. C-AFM current images revealed the difference in charge transport behavior of the core and shell moieties.
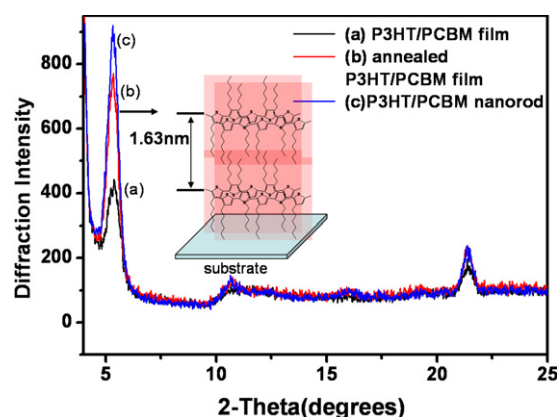
Acknowledgments

Appendix

Figure A.1. Grazing-incidence XRD diffraction diagrams of P3HT/PCBM(1:1, w/w) as-cast films, identically annealed at 120°C for 10 min and P3HT/PCBM nanorod structure. The increase at $2\Theta \sim 5°$ (interchain distance of interdigitated alkyl chain in P3HT) and $2\Theta \sim 22°$ (interchain distance of face-to-face packing of the thiophene ring) is observed. That means crystallinity is improved.

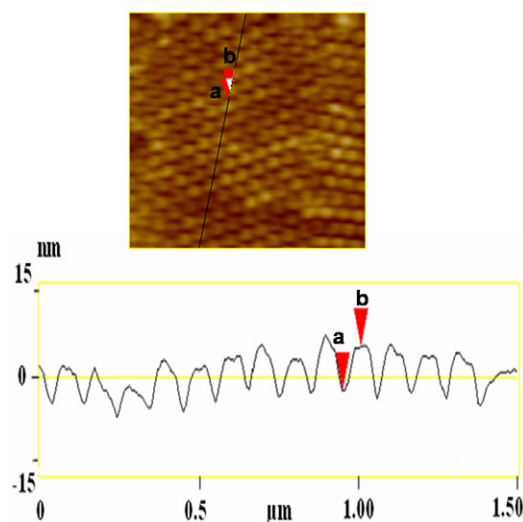**Figure A.2.** Atomic force microscopy (AFM) topographic images for of a thin film P3HT/PCBM nanorod structure. The image size is 1.48 μm × 1.48 μm and the vertical scale is 70 nm.
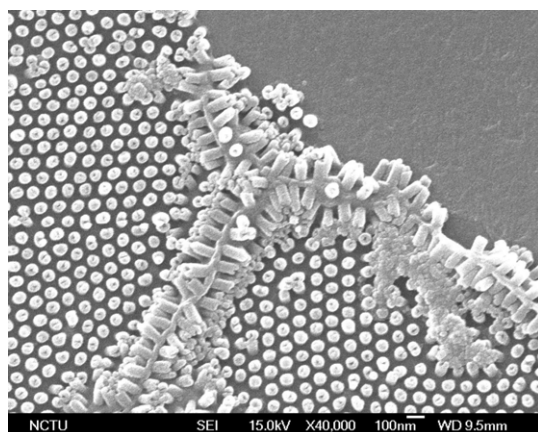

Figure A.3. Scanning electron microscopy (SEM) images of the P3HT/PCBM nanorod nanostructures. The length of the rod is 110 nm.

References

[1] Yu G, Gao J, Hummelen J C, Wudl F and Heeger A J 1995 *Science* **270** 1789

[2] Yu B Y, Tsai A, Tsai S P, Wong K T, Yang Y, Chu C W and Shyue J J 2008 *Nanotechnology* **19** 255202

[3] Dridi C, Barlier V, Chaabane H, Davenas J and Ouada H B 2008 *Nanotechnology* **19** 375201

[4] Ma W, Yang C, Gong X, Lee K and Heeger A J 2005 *Adv. Funct. Mater.* **15** 1617

[5] Kwong C Y, Choy W C H, Djurisic A B, Chui P C, Cheng K W and Chan W K 2004 *Nanotechnology* **15** 1156

[6] Chang Y T, Hsu S L, Su M H and Wei K H 2007 *Adv. Funct. Mater.* **17** 3326

[7] Chang Y T, Hsu S L, Chen G Y, Su M H, Wei K H, Singh T A and Diau E W G 2008 *Adv. Funct. Mater.* **18** 2356

[8] Kim J Y, Lee K, Coates N E, Moses D, Nguyen T Q, Dante M and Heeger A J 2007 *Science* **317** 222

[9] Li G, Shrotriya V, Huang J, Yao Y, Moriarty T, Emery K and Yang Y 2005 *Nat. Mater.* **4** 864

[10] Hadipour A, Boer B D and Blom P W M 2008 *Adv. Funct. Mater.* **18** 1

[11] Thompson B C and Frechet J M 2008 *Angew. Chem. Int. Edn* **47** 58

[12] Chen J T, Zhang M and Russell T P 2007 *Nano Lett.* **7** 183

[13] Steinhart M, Wehrspohn R B, Gosele U and Wendorff J H 2004 *Angew. Chem. Int. Edn* **43** 1334

[14] Zhang M, Dobriyal P, Chen J T and Russell T P 2006 *Nano Lett.* **6** 1075

[15] Lee S H, Park D H, Kim K and Joo J 2007 *Appl. Phys. Lett.* **91** 263102

[16] Coakley K M, Srinivasan B S, Ziebarth J M, Goh C, Liu Y and McGehee M D 2005 *Adv. Funct. Mater.* **15** 1927

[17] Reid O G, Munechika K and Ginger D S 2008 *Nano Lett.* **8** 1602

[18] Chiu M Y, Jeng U S, Su C H, Liang K S and Wei K H 2008 *Adv. Mater.* **20** 2573

[19] Mihaiketchi V D, Xie H, Boer B D, Koster L J A and Blom P W M 2006 *Adv. Funct. Mater.* **16** 699

[20] Duche D, Escoubas L, Simon J J, Torchio P, Vervisch W and Flory F 2008 *Appl. Phys. Lett.* **92** 193310